

Review

Fatigue Assessment of Wind Turbine Towers: Review of Processing Strategies with Illustrative Case Study

João Pacheco, Francisco Pimenta , Sérgio Pereira, Álvaro Cunha  and Filipe Magalhães * 

Construct-ViBest, Faculty of Engineering (FEUP), University of Porto, 4200-465 Porto, Portugal; up201104344@edu.fe.up.pt (J.P.); ec09176@fe.up.pt (F.P.); sbp@fe.up.pt (S.P.); acunha@fe.up.pt (Á.C.)

* Correspondence: filipema@fe.up.pt

Abstract: Wind turbines are structures predominantly subjected to dynamic loads throughout their period of life. In that sense, fatigue design plays a central role. Particularly, support structure design might be conservative with respect to fatigue, which may lead to a real fatigue life of considerably more than 20 years. For these reasons, the implementation of a fatigue monitoring system can be an important advantage for the management of wind farms, providing the following outputs: (i) estimation of the evolution of real fatigue condition; (ii) since the real condition of fatigue damage is known, these results could be an essential element for a decision about extending the lifespan of the structure and the possibility of repowering or overpowering; and (iii) the results of the instrumented wind turbines can be extrapolated to other wind turbines of the same wind farm. This paper reviews the procedures for calculating the fatigue damage of wind turbine towers using strain measurements. The applicability of the described procedures is demonstrated with experimental data acquired in an extensive experimental campaign developed at Tocha Wind Farm, an onshore wind farm located in Portugal, exploring the impact of several user-defined parameters on the fatigue results. The paper also includes the description of the data processing needed to convert raw measurements into bending moments and several validation and calibration steps.

Keywords: wind turbine; fatigue assessment; dynamic monitoring; strain gauges



Citation: Pacheco, J.; Pimenta, F.; Pereira, S.; Cunha, Á.; Magalhães, F. Fatigue Assessment of Wind Turbine Towers: Review of Processing Strategies with Illustrative Case Study. *Energies* **2022**, *15*, 4782. <https://doi.org/10.3390/en15134782>

Academic Editors: Francesc Pozo and Yolanda Vidal

Received: 25 May 2022

Accepted: 24 June 2022

Published: 29 June 2022

Publisher's Note: MDPI stays neutral with regard to jurisdictional claims in published maps and institutional affiliations.



Copyright: © 2022 by the authors. Licensee MDPI, Basel, Switzerland. This article is an open access article distributed under the terms and conditions of the Creative Commons Attribution (CC BY) license (<https://creativecommons.org/licenses/by/4.0/>).

1. Introduction

Fatigue is defined as a physical phenomenon where a material cracks after bearing a certain number of load cycles, whereas a single load of the same magnitude would not have caused a failure [1,2]. This is a common cause of failure in structures and components subjected to time-variable loadings, such as wind turbines.

Fatigue design of wind turbines is actually a very complex task. On the one hand, wind turbines are composed by large structural components designed with several materials, leading to different properties and assessment procedures [3]. On the other hand, the definition of the loading scenarios is a difficult and extensive task. It is important to note that, apart from quasi-static loads, wind loads have a considerable uncertainty in their quantification because of their dynamic and non-deterministic nature.

In general, two distinct approaches in fatigue analysis can be followed [4]: (a) use the cumulative fatigue damage to predict fatigue life, assuming that a failure occurs after a number of loading cycles at a particular tension/stress range; and (b) examine the fracture behavior of mechanical elements under dynamic loads and consider that a failure occurs if the remaining strength of the component is insufficient because of cracks that have grown to a critical length. Although the second method is more accurate for fatigue life prediction, it is not commonly used because crack behavior models are more complex to determine.

In a very simple way, following the first approach, the fatigue assessment consists of a determination of the loading history, the identification of the damage cycles, and the estimation of the total fatigue damage by aggregating the damage contributions of

each damage cycle. In time domain analysis, the structure response is expressed as a stress or strain history and fatigue damage occurs as a result of stress/strain variation over time (so-called cycles). The damage is estimated according to the hypothesis of linear damage accumulation, the so-called Palmgren–Miner rule [5]. A simple description of how fatigue damage accumulates in a structural component is provided in [6]. According to Wöhler, each cycle of constant stress range causes a certain amount of damage and that damage increases linearly with the number of stress cycles applied, until the material breaks. The parameters that may influence fatigue strength are the stress range and the average stress associated with each cycle. A complete description of this procedure is presented in Section 2 of this paper.

Alternatively, frequency-domain methods might be applied. As mentioned above, wind turbines are exposed to random loads that translate into an equally random response. In reality, these response stresses and input loadings can be viewed as the realization of a random Gaussian process that can be described in the frequency domain by a power spectral density (PSD) function. The PSD represents the distribution of the signal energy at different frequencies and it can be obtained with the application of fast Fourier transforms to the time signals. These transformations of loading time histories between time and frequency domain is subject to certain requirements, as the signal must be stationary and Gaussian (normal probability distribution).

The frequency-domain methods for fatigue assessment offer a direct connection between the PSD and damage or the cycle distribution of the loading. These methods can be divided into narrow-band and wide-band processes. A description of the fundamental theories of random vibration and of the methods to predict fatigue damage from a PSD of stress response are introduced [7]. In a general way, for a narrow-band process, it is reasonable to assume that every peak of the PSD is coincident with a cycle and that the cycle amplitudes are Rayleigh-distributed, although for a wide-band process the relation of the peak distribution and cycle amplitudes is much more complex and several empirical solutions have been proposed [8–10].

Frequency-domain methods for dynamic and fatigue analysis have been widely used in the offshore oil and gas engineering field. In [11], the fatigue assessment with a frequency-domain approach of a bottom-fixed monopile turbine was performed. An acceptable accuracy compared to time-domain numerical simulations and full-scale measurements was found. Other studies applying frequency-domain analysis for wind turbines have been reported in [12,13].

Regarding the classical approach combining S-N curves and a rainflow counting algorithm, it is important to mention some limitations of this method [14]. As a result of improved manufacturing processes, the steel currently used in the construction of the towers has more advanced properties than the material used in the tests on which the S-N curves are based. On the other hand, this method does not allow consideration of the sequential effect of the stress history. It is verified that the crack opening speed is related to the chronological order of the load cycles, which cannot be done with linear damage accumulation. Finally, this method neglects the material's ability to regenerate, since cracks may have the ability to heal when subjected to compressive stresses.

Despite the limitations of the classic approach, the combination of rainflow counting and the Palmgren–Miner rule has been tried and tested thoroughly and is generally accepted as one of the best time-domain methods for a fatigue-life estimation. The main standards and guidelines of wind turbines, including IEC 61400-3 [15], IEC 61400-1 [16], DNV-2011 [17], GL-2010 [18], and GL-2012 [19], suggest the application of the linear accumulation of damage for fatigue analysis of the support structure.

One of the first examples of fatigue assessment of a wind turbine tower based on the measurement of strains is described in [20]. The experimental campaign lasted nine months and included the installation of four sensors in a 500 kW rated power onshore wind turbine. The collected data was processed with the application of the rainflow counting algorithm. This work was intended to optimize the design of these structures.

Within the scope of the “high-strength steel tower for wind turbines” project, a 2.1 MW wind turbine located in Portugal was instrumented with 96 strain channels [21]. The main goal of the project was to improve the competitiveness of the steel towers used to support multi-megawatt wind turbines.

Pollino and Huckelbridge [22] monitored a 100 kW wind turbine with strain gauges over approximately one year and concluded that the fatigue life of the principal structural details of the tower was significantly higher than 20 years.

To study in detail the connection between the steel tower and the concrete foundation, a monitoring system based on accelerometers and strain measurements was deployed in a wind turbine located in south Germany [23].

More recently, Weijtens [24] describes an experimental campaign carried out in the North Sea under the Northwind offshore wind project. The Northwind farm comprises 72 Vestas V112-3MW offshore wind turbines (monopile foundations) with a 216 MW capacity and started operation in 2014. This work presents the fleet leader concept, in which a limited number of representative wind turbines are instrumented with strain gauges and accelerometers (two wind turbines were instrumented in this case). The fatigue damage on the two wind turbines is quantified keeping in mind the prediction of the fatigue-life progression in the entire wind farm.

A long-term monitoring system for structural and fatigue verification of wind turbine support structures is presented in [25]. The monitoring system is installed on a Vestas V90-2.0 MW wind turbine situated in the biggest wind farm of Switzerland (Mont-Crosin, BE). The results of this work demonstrated that the wind turbine tower service duration could be extended safely beyond 20 years using simple monitoring systems.

All these works prove the relevance of fatigue assessment of wind turbines with dynamic monitoring systems based on strains measurement. This paper seeks, in a pedagogical way and supported by a practical case study, to evaluate the impact that different variables can have on the final calculation of fatigue in wind turbine towers. In fact, in the performed literature review, no relevant contributions were found that sought to jointly assess the impact of the various variables considered in this work, using a sufficiently large amount of experimental data collected in a utility-scale modern wind turbine. Most of the results found are based on numerical modeling or experimental work carried out on older and outdated models of wind turbines.

This paper is organized as follows: Section 2 gives the background of the procedure for calculation of fatigue damage on wind turbine towers based on strain measurements. Some shortcomings of this approach and alternatives are also presented and discussed.

The case study of the Tocha Wind Farm is introduced in Section 3, as well as the experimental monitoring campaign. Results from a two-year measurement campaign in Tocha Wind Farm will be used.

In a first step, the experimental determination of bending moments at the tower requires the acquired raw strain data to be preprocessed to obtain the actual deformation (described in Section 4). Thus, special attention is given to strain-signals processing, which includes temperature effects compensation and signal calibration according to IEC 61400-13. Advanced numerical models of the wind turbine are also being developed in FAST [26]. The experimental tower bending moments reported in this contribution are compared with their numerical counterparts.

Afterward, fatigue assessment based on rainflow counting and the Palmgren–Miner rule can be performed. An estimation of the damage accumulated over the monitoring period is obtained. The sensitivity of the calculated fatigue damage to several parameters (window length of strain time series, rainflow histogram resolution, S-N curve parameters, and strain-signal sampling frequency) is evaluated (Section 5).

Finally, the conclusions and future developments are given in Section 6.

2. Fatigue Assessment Using Strains Gauges

The fatigue damage calculation procedure based on strain measurements involves a significant number of processing steps. An overview of this procedure is given in Figure 1. All the involved steps are described in this section and most of them are then illustrated in a case study.

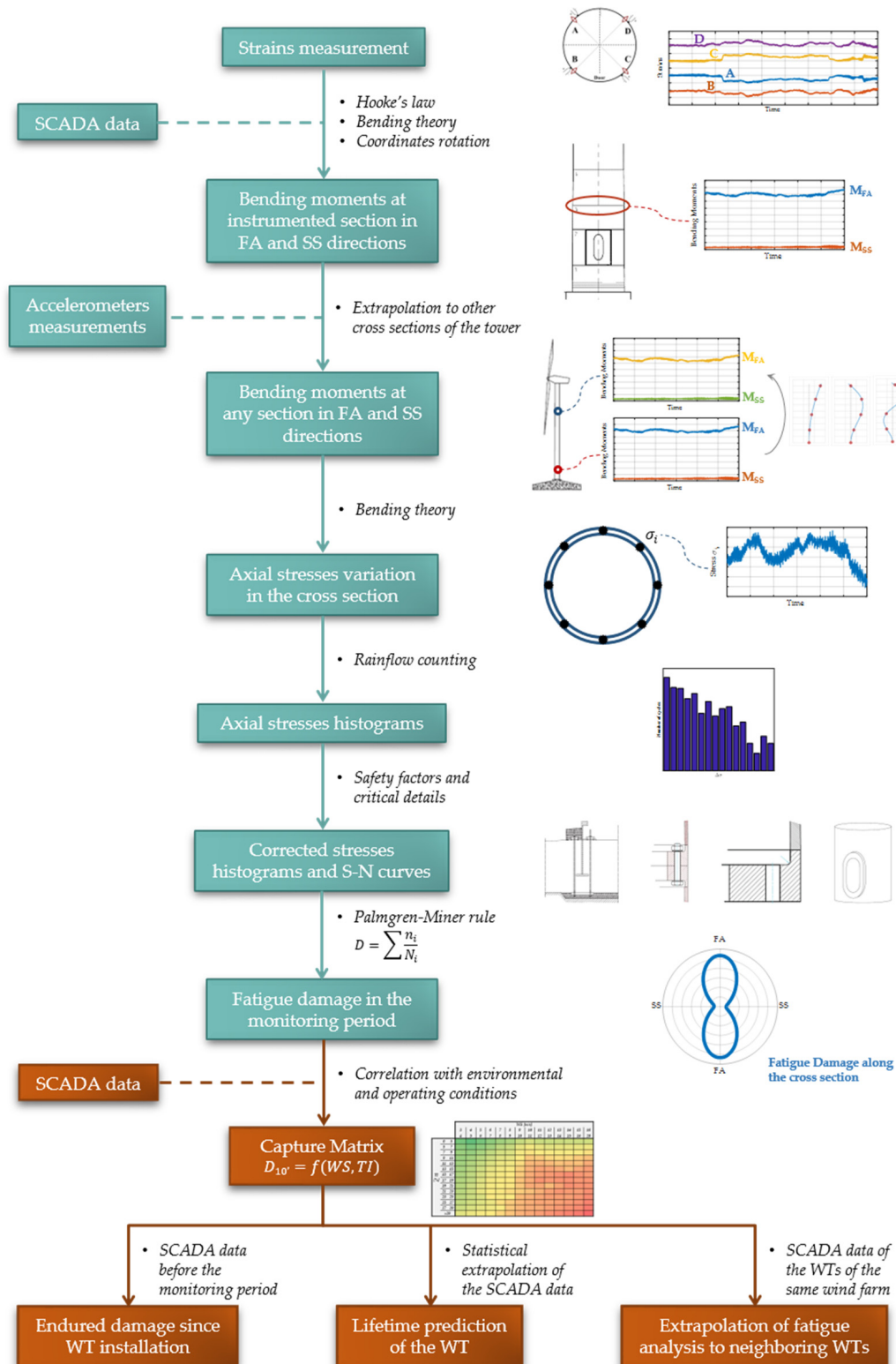


Figure 1. Fatigue assessment procedure based on strain measurements.

2.1. Bending Moments at Instrumented Section

The longitudinal strain signals (ε_z) are the input of this procedure. According to the theory of linear elasticity (Hooke's law) for isotropic materials, the longitudinal stress in the tower (σ_z) is given by:

$$\sigma_z = E \cdot \varepsilon_z \quad (1)$$

where E is the Young's modulus of the steel. It is important to note that the previous equation is valid since the radial deformations caused by the thrust force are negligible when compared to the longitudinal deformations, considering the small thickness of the tower cross-sections.

The calculated stress at any sensor installed in the cross-section results from the combination of two bending moments in two perpendicular directions (M_x and M_y) and the normal force (F_N), according the following equation:

$$\sigma_z(\theta_i) = \frac{M_x}{W} \cdot \cos(\theta_i) - \frac{M_y}{W} \cdot \sin(\theta_i) + \frac{F_N}{A}, \quad i = \{1, 2, 3, \dots\} \quad (2)$$

where θ_i is the angle of the i -th sensor from the x -axis aligned with the door and A and W are the cross-section area and the elastic section modulus, respectively. To calculate the normal force and the two bending moments installed in the cross-section, it is required to measure the longitudinal stress at, at least, three different locations. As the strain sensors only provide the variation from the initial stress state of the structure, the normal force resulting from the tower, nacelle, and rotor weight cannot be measured. Still, this can be easily estimated if all the supported masses are known.

In fact, the relevance of mean stress in fatigue analysis in the standards and guidelines depends on the structural detail under analysis. For the fatigue analysis of concrete elements (i.e., foundations and grouted joints) or preloaded bolted joints, the knowledge of the mean stress is required [27]. For the analysis of the steel elements of the support structure, some standards and guidelines present a correction coefficient to consider the mean stress effect. However, it is usually disregarded because its consideration introduces a positive effect when the stress range is in the compression side. Thus, it is conservative to neglect this coefficient and, consequently, the mean stress effect.

The nacelle orientation defines the fore-aft (FA) and the perpendicular side-to-side (SS) direction. Subsequently, the bending moment with a vector perpendicular to the rotor axis (M_{FA}) and the perpendicular direction moment (M_{SS}) are obtained by projecting the M_x and M_y bending moments using the yaw angle provided by the SCADA system.

2.2. Extrapolation of the Bending Moments

2.2.1. Critical Construction Details

Due to its geometry and construction process, the wind turbine structures have several details that need to be verified against fatigue damage. Considering only the support structure of onshore wind turbines (tower and foundation), there are mainly five spots of interest: the flange connection between tower segments (including the bolts), the vertical and horizontal welded connections between the tower cylindrical sheets, the welded connections between the tower cylindrical sheets and the flange, the stress concentration that is due to the door opening, and the connection between the tower and the foundation.

The flanged connection between the tower segments results in an eccentrically loaded bolted connection. In this way, a fast bolt-fatigue failure can occur when the external loads are high relative to the bolt preload because the eccentricity of the connection results in a nonlinear relationship between the tensile forces in the bolt and the load applied to the structure.

Some bolted connection designs are described in [28] and different models to estimate the load transferred into bolts can be found in the guideline [29]. Pedersen [30] concludes that the bolted connections can be optimized by placing the bolts as close as possible to the

tower wall (to reduce the eccentricity) and also demonstrated that an increase in the flange thickness can reduce the stresses in the bolts.

Although it is important to note that during the normal operation of the wind turbine, the stress variation inside the prestressed bolts is low and the opening of the joints is not expected [21]. A correct maintenance program for this type of connection makes it possible to correct prestressing losses and prevent possible damage to the structure.

Damage in onshore wind turbine support structures is usually related to foundation problems and the connection between the tower and the foundation is a sensitive location for fatigue [31]. Some problems of excessive levels of vibration have been observed because of the cracking and/or gaps in the concrete around the steel ring embedded in the foundation [32].

For offshore bottom fixed turbines, other locations are very sensitive for fatigue damage: in mono-piles the grouted connection of the transition piece is particularly sensitive and foundation models like tripods and jackets present complex geometries with a high number of joints with high stress concentrations.

The design codes present rules that permit the conversion of the stress observed in a current cross-section to the ones applied in the critical spots of common details (using detail categories as referred to in Section 2.5). If this is not available, local detailed finite elements models have to be constructed.

2.2.2. Extrapolation of the Bending Moments to Non-Instrumented Sections

For the complete evaluation of the fatigue damage, it is essential to know the distribution of stresses or strains along the structure, in particular at the critical positions identified in the previous section. However, at many critical details, or cross-sections close to the critical details, direct measurements of strains are not feasible. It might be impossible because of difficulties to access these cross-sections and also because the instrumentation of all critical spots is not economically feasible.

Thus, when direct measurements of strains are not available, the fatigue assessment of a wind turbine spot can be performed: (a) through estimation of the dynamic loads applied to the structure, or (b) through model-based extrapolation of a limited set of available response measurements.

The first method allows the reconstruction of the dynamic loads applied to the structure. Many algorithms for force identification can be found in the literature [33–35], which already had practical applications in wind turbines. Fritzen in his works adopted a robust observer technique for estimating the wind loads on a 5 MW wind turbine [36].

Alternatively, response estimation techniques can be used to estimate the strains at any fatigue location without the necessity of prior sensor installation on these locations. From the obtained stress histories, the consumed fatigue can be assessed. This so-called virtual sensing concept utilizes a limited set of response measurements, as accelerations, strains, or SCADA data, to reconstruct the full-field response of the structure.

Various approaches for the estimation of stresses and strains using response estimation techniques are presented in the literature. These virtual sensing techniques can be divided into: the model-based robust observers [37,38], the Kalman filter-based techniques, the joint input-state filtering techniques, and model decomposition and expansion technique (briefly introduced next). The joint-state input estimation was proposed by Gillijns and Moor [39] and further developed by Lourens et al. [40]. This method estimates the loads and states of the structural model based on filtering. Posteriorly, this algorithm was extended to be applied when accelerations are measured [41]. Similarly, the Kalman filter-based techniques estimate states based on a limited number of response measurements. This approach was introduced to be applied to structural dynamics by Papadimitriou et al. [42]. The Kalman filters have proven effective on the simultaneous integration of multiple types of measurements (e.g., accelerations and strains measurements) [43,44]. Alternatively, model decomposition and expansion technique assume structural response as a linear

combination of the mode-shape vectors [45]. Modal expansion algorithms can be applied both in time and frequency domains [46–48].

A comparison of the applicability in offshore monopile wind turbines of the Kalman filter, joint input-state filter and modal expansion is carried out in [49], which concludes on an acceptable performance in the prediction of acceleration responses in offshore wind turbine foundations.

The fatigue condition in an arbitrary position of the wind turbine structure can be obtained as the sum of the contribution of two components: quasi-static and dynamic. The quasi-static component corresponds to the stress conditions associated with the lower frequency range of the spectrum, generally related to the quasi-static component of the wind action, while the dynamic fatigue component corresponds to the stress conditions associated with higher frequencies of the structure response, which includes the contribution of sinusoidal excitations and vibration modes.

In a simplified way, the quasi-static component of fatigue can be determined by knowing the configuration of the global deformation of the structure and the quasi-static condition at a reference point. The deformed shape of the structure can be estimated based on its stiffness matrix and knowing the most common loading configuration. The quasi-static reference condition can be a bending moment (measured with strain gauges), the evolution of a displacement (measured with GPS), or curvature (measured with inclinometers) over time in an appropriate section of the structure. Assuming the deformed configuration of the structure and a known reference condition, the bending moment of the quasi-static component, and consequently the stresses, can be extrapolated for the entire structure.

Estimating the dynamic contribution to fatigue is a more complex task. In the works [45,50], a possible strategy is presented and exemplified. From the modal analysis carried out in the damage detection module, it is possible to determine the modal accelerations of the structure. Adopting a double integration process, the corresponding modal displacements can be determined. Knowing the displacement field for each vibration mode, it is possible to calculate the equivalent forces that impose the same modal deformation. Thus, the bending moment at any point in the structure is then obtained by summing up the bending moment contribution of each mode of vibration, once the partial contribution of each mode to the response of the structure is known.

2.3. Axial Stress Variation in the Cross Section

Considering only the stress variation along the FA and SS directions to determine the accumulated fatigue damage in the tower cross-sections is a conservative approach usually adopted in design, since it adopts a single dominant wind direction. To optimize the material capacity, the damage can be estimated over the section of the tower using the stress signals calculated along the perimeter of the cross-section (for example, every 10°).

In this way, the cross-section is divided in segments and the stresses at each central point are calculated knowing the geometric characteristics of the section and the FA and SS bending moments.

2.4. Rainflow Counting

The rainflow cycle-counting algorithm translates the hysteresis loops experienced by the material during the loading history into a stress histogram. It gives the number of experimental cycles (n_i) for a certain stress range of the i -th bin ($\Delta\sigma_i$) of the factored stress spectrum.

The most common cycle counting methods are level crossing [51], peak cycle [52], and rainflow cycle counting [53]. The last method is indicated by Eurocode 3 for evaluation of the stress history and in [54] it is considered as the most accurate method among the other common methods.

The rainflow counting algorithm was developed by Matsuishi and Endo [55] and later Rychlik [56] gave a mathematical definition for the rainflow counting method. A num-

ber of variations of this original scheme have been published for various applications [57,58]. The biggest advantage of this method is that it accounts for all the peaks without doubling, thus there are no more drop-outs in the calculation in terms of uncounted small amplitudes, which leads to a less conservative estimation of the fatigue damage. Another major advantage of this method is that it allows the direct application of the Miner's rule to assess the fatigue life of a structure being subjected to a complex loading record.

The rainflow cycle counting of the stress is performed for both directions (FA and SS directions). The number of required stress bins must be preliminarily evaluated for each application. In IEC 61400-13 [59], it is indicated that to achieve sufficient resolution, the number of divisions of the load range shall be at least 100. However, in DNV GL AS [60], it is recommended that the number of bins should be large enough to ensure reasonable accuracy, and should not be less than 20.

2.5. Fatigue Damage during the Monitoring Period

Before calculating the fatigue damage on the structure, it is important to note that the nominal stresses obtained at the position of interest are associated with some uncertainty. To take into account the uncertainties about material properties and loads, and the consequences of failure, and to get a representative value for the concentrated stresses at specific details, the standards and guidelines also define partial safety factors.

For example, Eurocode 3 defines a partial factor for the equivalent constant amplitude stress range (γ_{Ff}), which must be multiplied by the stress differences ($\Delta\sigma_i$) obtained from a load spectrum, and the stress strength ($\Delta\sigma_c$) is divided by the partial factor for fatigue strength (γ_{Mf}). These partial safety factors are applied separately to loads and resistances to obtain the required safety level. On the other hand, [61] indicates an overall safety factor (SF) obtained by multiplying several sub-factors, such as the stress concentration factor, size effect correction, and material safety factor.

Still other factors must be considered for each practical application. In [62], two types of adhesions for the strain gauges were compared: strain gauges were glued to the turbine wall or welded to the steel. In this study, fiber Bragg gratings (FBGs) were used. A 10% reduction in sensitivity was observed for the welded strain gauges compared to the glued strain gauges.

In the last step, the damage calculation is based on the assumption of linear damage accumulation of each stress cycle, according to the Palmgren–Miner rule. The total fatigue damage (D_{total}) is given by:

$$D_{total} = \sum_j \sum_{i=1}^{n_\sigma} \frac{n_{ij}}{N_i} \quad (3)$$

where indices i and j correspond to the i -th stress bin of the j -th time series. The n_{ij} is the number of cycles associated with the stress range $\Delta\sigma_i$ and N_i represents the number of cycles to failure at a constant stress range σ_i , which it is obtained from the corresponding S-N curve.

The S-N curves represent the fatigue resistance of a given detail and are determined from series of fatigue tests on laboratory specimens. Typically, these curves are associated with a given survival probability and level of confidence. For the design of steel support structures, all the standards and guidelines define similar S-N curve equations for fatigue analysis. For example, for components predominantly loaded by normal stress, the guideline GL-2010 [18] recommends the same bilinear S-N curves as defined in Eurocode 3, but disregards the threshold value of fatigue strength. The GL-2010 [18] do not recommend the use of an endurance limit. Figure 2 represents the S-N curves provided by the two references for a particular detail.

It is important to note that Eurocode 3 defines partial safety factors to be applied to the fatigue strength curves according to the accessibility of the component during periodic inspection and maintenance, and the consequences of failure. A full description of the S-N curves of the different codes and a comparative study of these curves can be found in [63].

In conclusion, the calculated damage refers to the degree of damage of the material under cyclic loading and it is represented by a dimensionless parameter D . If $D = 0$ the material is considered intact and if $D > 1$ the material has reached its fatigue life.

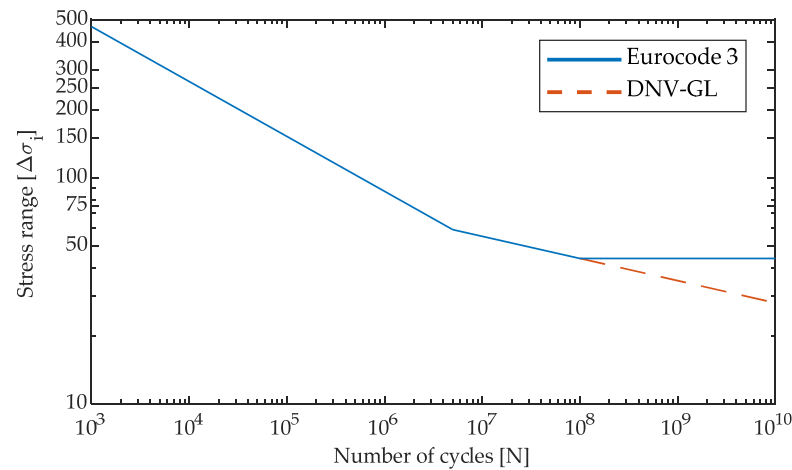


Figure 2. S-N curves defined in GL-2010 and Eurocode 3 (category detail 80 MPa).

2.6. Extrapolation of the Fatigue Damage in Time

Direct measurement of strains at the wind turbine tower allows us to estimate the accumulated fatigue damage with good accuracy over the monitoring period. This is an important source of information that can be used to estimate the damage prior to and after the monitoring period. The main goal is to estimate the damage at a given angle of the tower section based on a few data from the SCADA system: wind speed, turbulence intensity, and yaw angle (nacelle orientation).

The presented strategy combines a period of measurements with strains with long-term SCADA data. The experimentally estimated damage (e.g., 10 min damage values) are first clustered into several load cases (e.g., power production, parked/idling, and emergency shutdown). Based on the approach described in IEC 61400-13 [59], the damage values are stored in a database according to the corresponding wind speed and turbulence intensity, the so-called capture matrix. If the wind turbine is directly in the wake of neighboring wind turbines along the main wind direction, the IEC 61400-13 recommends classifying the damage according to the turbulence intensity and the wind sector. This is illustrated by Weijtens et al. [24], who performed the damage estimation of an offshore wind turbine taking in account the variation of the turbulence intensity with respect to the wind sector.

For each 10 min time series, a damage value ($D_{10'}$) is picked from the capture matrix bin according to the wind speed (WS) and turbulence intensity (TI) given by the SCADA system before the monitoring period. The sum of all individual damage results in the endured damage ($D_{endured}$) over the cross-section of the tower for the period with available SCADA data is:

$$D_{endured} = \sum D_{10'}(WS, TI) \cdot rot(Yaw) \quad (4)$$

where $rot(Yaw)$ represent a rotating matrix taking into account the wind direction. Note that the endured damage is calculated over the cross-section of the tower. In the previous equation, the term " $rot(Yaw)$ " aims to take into account the nacelle orientation (yaw angle) and the referential defined for the strain gauges.

The total endured damage may then be used to estimate the remaining useful lifetime (RUL) of the structure. In a direct way, considering the past period (with available SCADA data) as representative of the whole period of life, the RUL is obtained as:

$$RUL = \frac{T_{operating}}{D_{endured}} - T_{operation} \quad (5)$$

where $T_{operation}$ represents the number of years since the wind turbine started operation (assuming SCADA data are always available).

It is important to note that this extrapolation assumes that the monitored period is representative of the loading scenarios from the whole period of operation of the wind turbine. Usually, one year is considered as the minimum monitoring period. Hübler suggests that strain measurements of about 9 to 10 months lead to a relatively representative and unbiased dataset for fatigue damage extrapolation on offshore wind turbines, referring to the higher time periods reducing the occurring errors only slightly [64], although a more complex approach, based on the probability distribution of environmental and operational conditions, can be followed, as shown in [11].

Finally, considering that similar wind turbines (same model, controller system, and similar loadings) have the same behavior in the wind farm, the damage capture matrix obtained for the instrumented wind turbine can be used for the other wind turbines in the same wind farm, adopting a fleet leader concept, as described in [24].

3. Description of the Case Study

In the previous section, the general procedure to calculate the fatigue damage was presented. However, for a better insight and validation of this procedure, measurement data are needed. In this work, measurement data of a large experimental campaign in Tocha Wind Farm are used. The results here presented were obtained from a database collected from February 2019 to April 2020.

3.1. Tocha Wind Farm

Tocha Wind Farm is located in the central region of Portugal, inserted in a coastal area with a plain sandy terrain. It consists of five VESTAS wind turbines, model V100 with 1.8 MW of rated power, totaling 9 MW of installed power. It is owned by EDP Renewables and started operation in May 2012. Figure 3a,b show, respectively, the geographic location of the wind farm and the distribution of the five wind turbines and the substation position, as well as a meteorological mast.

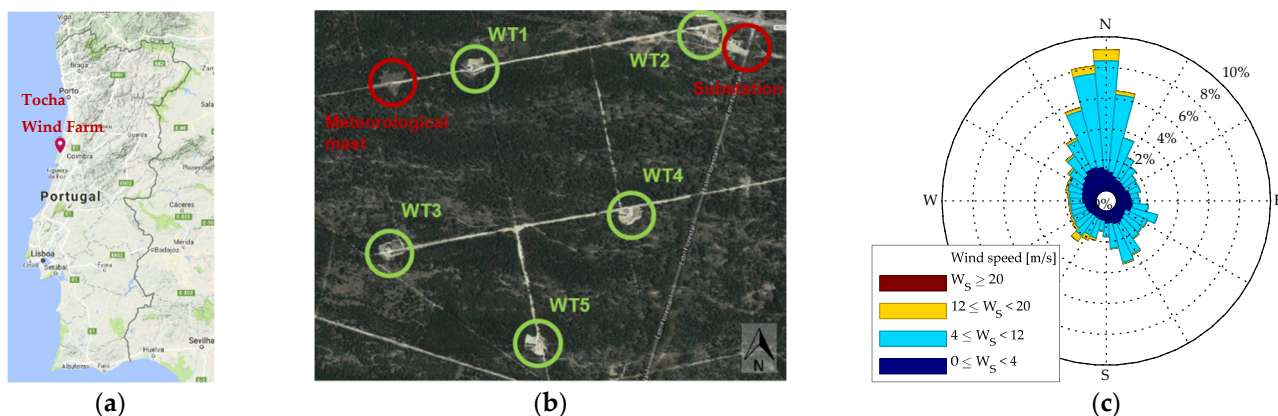


Figure 3. Tocha Wind Farm: (a) geographic location in Portugal; (b) wind turbines and auxiliary structures; and (c) characterization of the wind conditions observed between 2013 and 2018, based on data provided by meteorological mast (100 m high measurements).

The wind rose (Figure 3c) obtained with the wind measured at the meteorological mast between 2013 and 2018 reveals that the predominant wind direction is approximately north and it also reveals a secondary wind direction along the southeast direction. Thus, considering the very smooth terrain and the proximity of the coast, wind turbines 1, 2, and 3 are exposed to slightly disturbing offshore winds, while the remaining turbines are exposed to wind with additional turbulence caused by wake effects.

The Vestas V100-1.8MW is an onshore wind turbine model designed for low-wind onshore sites with a 100 m diameter rotor. It is a variable speed, three-blade, up-wind turbine

with individual pitch control for each blade. The wind turbine operates for wind speeds between 4 and 20 m/s and achieves the rated power for wind speeds of about 12 m/s.

The hub is placed at a height of 95 m and is supported by a steel tower, with a hollow circular cross-section of variable diameter and thickness and composed of four segments that are linked on site with bolted connections. Since the soil is sand, the steel tower is connected to a 14 by 14 m concrete slab supported by sixteen concrete piles with 1 m diameters.

3.2. Tower Monitoring System

Within the scope of the WindFarmSHM research project, the experimental campaign in the Tocha Wind Farm involves the simultaneous instrumentation of several wind turbines during a period of about two years, adopting three monitoring layouts (that include accelerometers, strain gauges, and clinometers distributed in the tower and blades). However, only the dynamic monitoring system of the tower accelerations and strains installed in wind turbine 1 are briefly described in this paper. A detailed description of the Tocha Wind Farm experimental campaign, as well as some preliminary results, can be found in [65].

3.2.1. Tower Monitoring System: Accelerometers

The acceleration measurement system installed in the tower is based on a central acquisition system to which all sensors are connected. It is composed of six force-balance accelerometers (Figure 4b) distributed along the tower height, measuring accelerations along two orthogonal horizontal directions at three sections, according to the scheme presented in Figure 4a. To limit the length of the GPS signal cable (the GPS antenna is located in the nacelle for time synchronization of the acquisition system), the central acquisition system is located at the top platform, about 87 m from ground level.

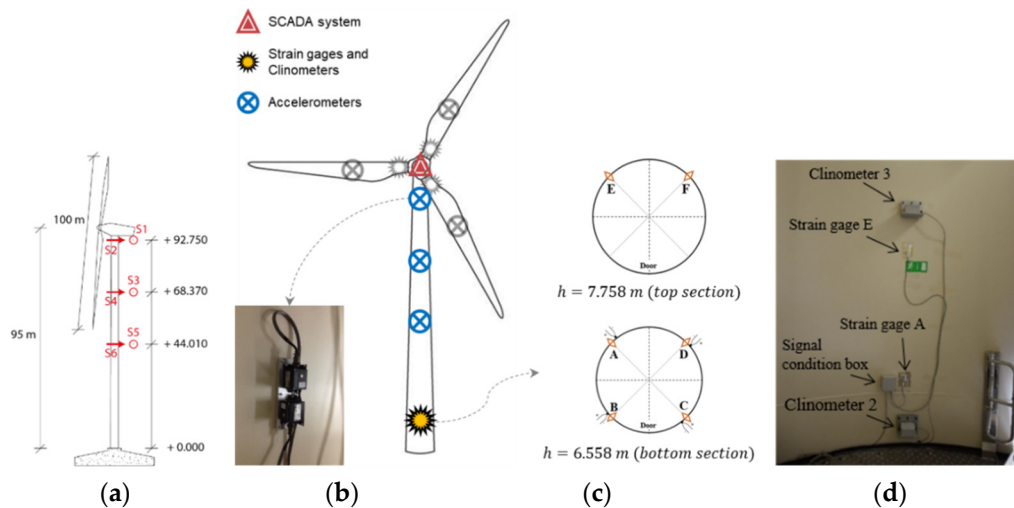


Figure 4. Tower monitoring systems: (a) sections instrumented with force balance accelerometers; (b) force balance sensors S1 and S2; (c) strain and rotation monitoring system; and (d) position of the strain gauges (\diamond) and temperature sensors (∇) at the tower.

3.2.2. Tower Monitoring System: Strains

The strain monitoring system is essential for fatigue assessment of the tower. It is composed of six 2D rosette strain gauges (measurement of the strain in two orthogonal directions) and four temperature sensors PT100. To try to evaluate the static bending moment diagram evolution along the tower, the six strain gauges are distributed in two sections: four sensors 6.5 m from the base of the tower (bottom section) and two sensors 7.7 m from the base of the tower (top section), as shown in Figure 4c,d. The four temperature sensors are located in the bottom section, close to the strain gauges.

Measuring deformation in the direction perpendicular to the tower axis, as well as temperatures, is important to allow the evaluation of alternative procedures to minimize the influence of temperature on the measured longitudinal deformations. Figure 4 also includes two clinometers, but the data collected by these sensors is not analyzed in this paper.

4. Experimental Evaluation of Bending Moments at the Tower

4.1. Data Synchronization

To process the data collected with the described monitoring system, it is essential to have SCADA data that accurately characterize the environmental and operational conditions of the wind turbine. In this study, the owner of the wind farm provides SCADA data with two types of sample rates of several operational and environmental parameters:

- SCADA-10min: these data are composed by the mean, maximum, and minimum value from a 10 min period of several operational and environmental parameters. Among them, the following were important in the context of this project: wind speed; wind direction; ambient temperature; rotor speed; yaw angle; blades pitch angle; and power output;
- SCADA high-resolution: data composed by the same parameters listed above, but with a sampling interval of 15 s.

The data acquired with a higher sampling frequency are very useful as they allow us to accurately monitor rapid variations of some parameters, such as wind speed (wind gusts of a few seconds), which is not possible to follow from the average values of the SCADA-10min.

As shown in Table 1, the tower monitoring systems is composed of three independent acquisition systems that adopt different timing protocols. In this way, it is necessary to synchronize all these systems in a common timeframe to permit the joint processing of different sensors datasets.

Table 1. Tower monitoring systems of wind turbine 1 and corresponding timing protocols.

Acquisition System	Sensors Type	Timing Protocols
KMI	Force-balance accelerometers	Global Positioning System time (GPS)
cRIO	Strain gauges Clinometers	Internal clock
SCADA	Temperature sensors SCADA sensors	Network Time Protocol (NTP)

The global positioning system time protocol was chosen as the reference from which all other systems were synchronized, so the force-balance accelerometer system gives the reference time. The synchronization of the cRIO acquisition system was performed by comparing the time series of strains with the time series of accelerations measured by the force-balance sensors, as shown in Figure 5. The delay between the two systems identified over time is variable because of the limited accuracy of the internal clock of the cRIO system, so the time shift between the two systems is continuously updated. In a second phase, to make this synchronization more accurate and easier to automate, a low-cost accelerometer placed next to an S6 force-balance sensor (Figure 4a) was connected to the cRIO system.

The synchronization of SCADA data was performed by comparing the evolution of the yaw angle (SCADA high-resolution) with the time series of strains over a full rotation of the nacelle. The eccentricity of the nacelle and rotor mass generates a sinusoidal signal in the strain gauges, as shown in Figure 6. A constant delay of approximately 50 s was observed between the two systems.

In the next subsections, the data processing needed to obtain an accurate experimental estimation of the bending moments based on strains measurements in the tower is briefly described.

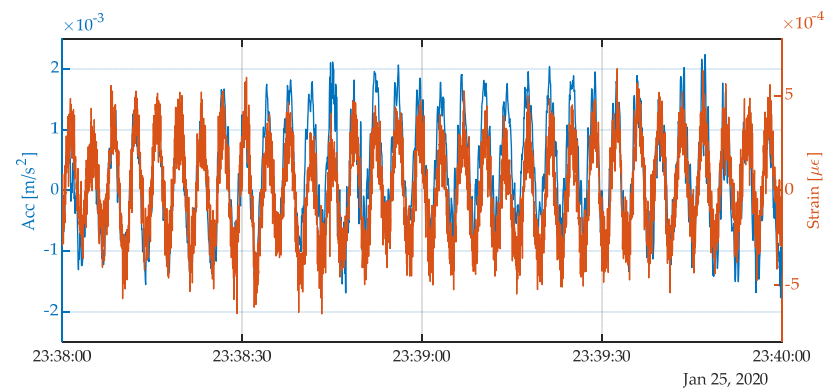


Figure 5. Synchronization of the KMI system (force-balance S3) and cRIO system (strain gauge B).

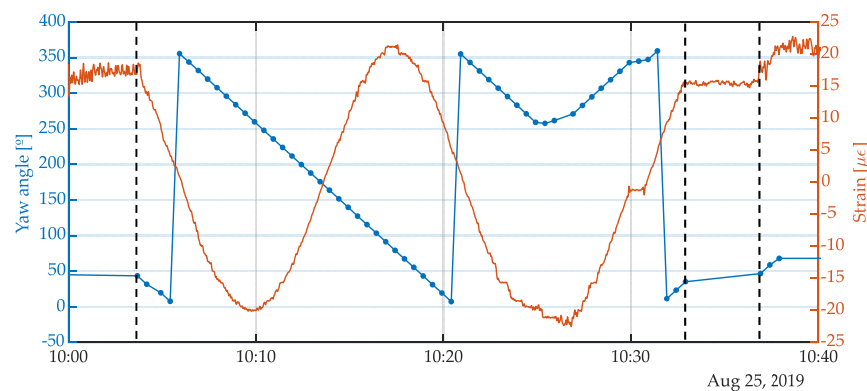


Figure 6. Synchronization of the SCADA data (yaw angle high-resolution) and cRIO system (strain gauge A) (the vertical dashed lines correspond to the singular points used for synchronization).

4.2. Compensation of Temperature Effects and Drifts

As a first step in the development of tools to assess the fatigue condition of wind turbine towers, this section describes the data processing needed to obtain an accurate experimental estimation of the bending moments applied in the tower of the fully instrumented wind turbine (WT1) of the Tocha Wind Farm and the validation of the obtained results using complementary monitoring components.

Strain gauges are very sensitive sensors and many factors can easily preclude accurate measurements. All potential sources of errors need to be identified and it is necessary to implement a methodology for the signal processing according to the precision of the intended results. Thus, the experimental determination of the bending moments in the tower requires the acquired raw data to be preprocessed to obtain the real deformation. In the present application, the methodology adopted consists of the following three steps:

1. Compensation of temperature effect on strain gauges;
2. Signal correction based on the signal average of diametrically opposed sensors;
3. Calibration check according to guideline IEC 61400-13 [59].

Many factors can easily distort strain measurements, but temperature is the most frequent source of errors. Temperature can influence the measurement of strains in two ways: thermal output and nonlinear temperature gradient. It should be noted that, in the installation under analysis, the strain gauges are connected to the acquisition system using a quarter-bridge configuration with three wires to avoid the effects of temperature on the cables.

Thermal output is caused by variation of the electrical resistivity of the grid conductor with temperature and the differential thermal expansion between the grid conductor and the steel of the tower. This effect is minimized using the thermal output compensation curve provided by the manufacturer and the temperature measured on the steel surface.

The local heating of the sun can also influence the measured strains, as the temperature gradient may become nonlinear. These parasite strains are minimized by averaging the two signals provided by the gauge couple installed at 180° .

A significant drift is observed on the strain signals over time [66]. The correction of this drift is based on the procedure defined by the IEC 61400-13 called calibration check. This procedure requires yawing the nacelle 360° below the cut-in wind speed, as shown in Figure 7a. The full rotation of the nacelle generates a sinusoidal signal because of the eccentricity of the nacelle and rotor mass, as shown in Figure 7b. If the effect of the axial force is disregarded, the mean of this signal represents the zero point. Please note that the strains presented in this figure were previously preprocessed to have zero mean.

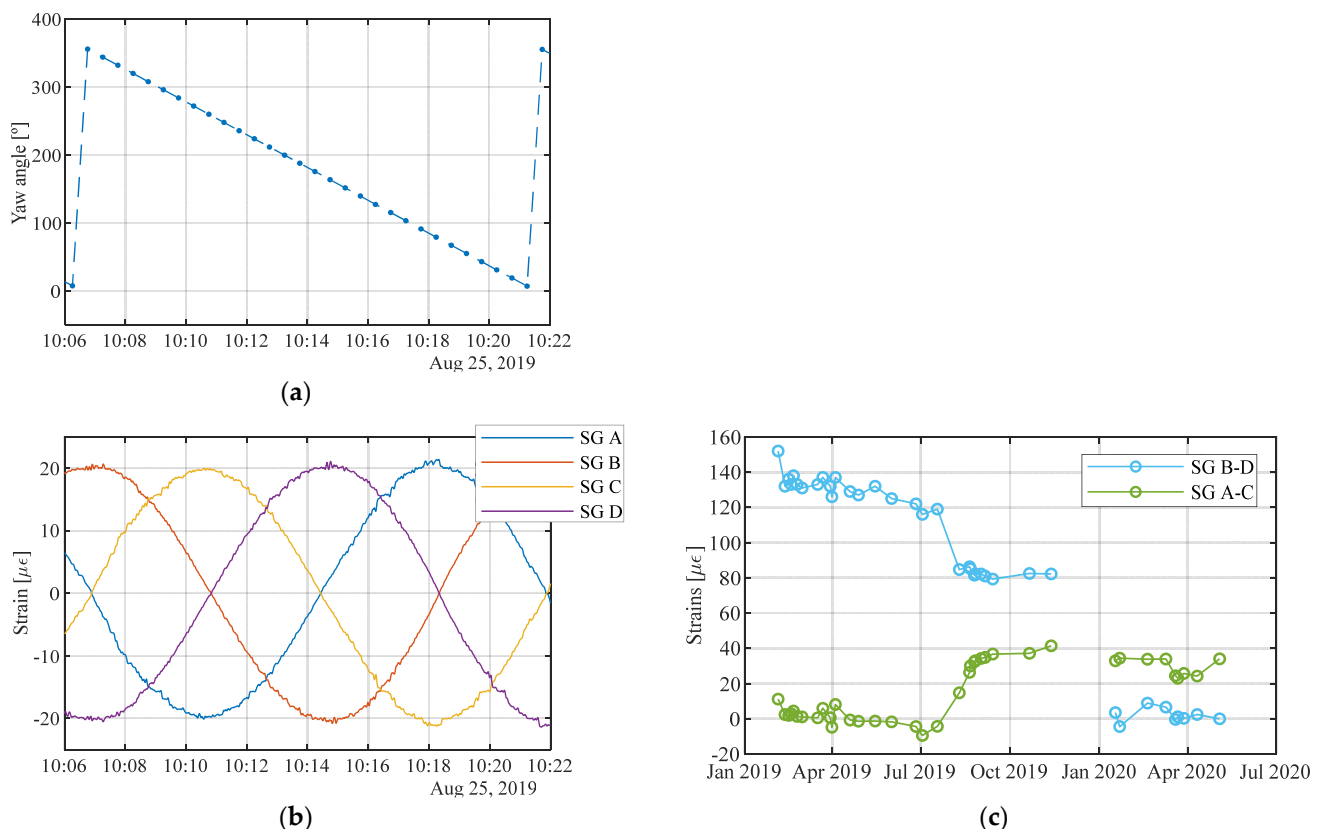


Figure 7. Strain-gauge calibration check: (a) yaw angle nacelle; (b) strain signals; and (c) mean value of the full rotation signals observed from February 2019 to April 2020 (see sensor positions in Figure 4c).

This procedure is also important to determine the exact position of the sensors in the instrumented section of the tower (despite the care used in the sensor gluing, there are always inaccuracies in sensor position). The value of the yaw angle for which the minimum value of the strain signals occurs is assumed to correspond to the radial position of each sensor. The nacelle angle defines the fore–aft and side–side directions for which the bending moments will be estimated.

A total of 38 full rotations of the nacelle, which met all the requirements, were observed in the period between 1 February 2019 and 30 April 2020 and were used for calibration (Figure 7c). In December 2019, there was a need to replace some components in the acquisition system that explains the sudden drift variation for the couple B-D. In the following months, the drift remains approximately constant.

4.3. Bending Moments Validation

To verify whether the values of the strains obtained based on the procedure described in the previous section correspond to real deformation of the structure that is due to the applied loads, some validation tests were performed.

In this sense, the average values of strains observed in all 10 min time series recorded (a total of 53,384 time series were collected in the monitoring period) are shown in Figure 8 as a function of the yaw angle. These values are compared with the theoretical strain curve that is obtained for the maximum thrust force applied at the rotor level (represented by the black curves). This theoretical curve was computed from the drag coefficients presented in [67].

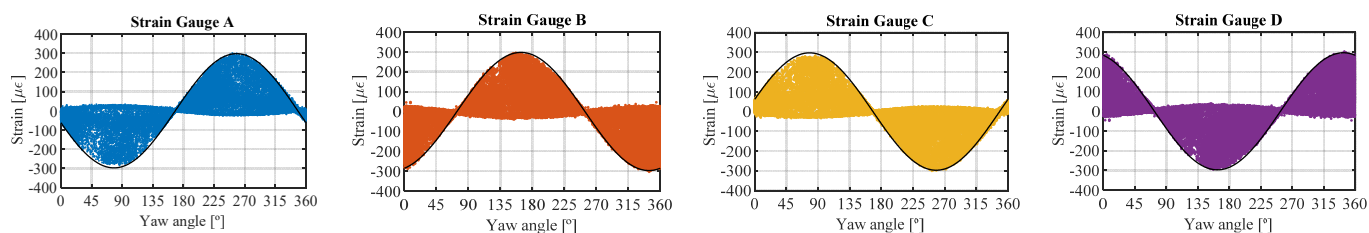


Figure 8. Ten-minute average strain signal of strain gauges A to D (see sensor positions in Figure 4c).

All the obtained experimental results (the cloud of points that almost completely fills the sinusoids) are well-framed by the theoretical curves. However, it should be noted that the maximum strain values are not obtained for all wind directions. This is because prevailing conditions of wind action exist. These results are also important to further validate the sensor positions.

In a second verification, the bending moments estimated from the measurement of strains were also compared with those that can be obtained from the measurement of accelerations. Considering a rotor stop event (in which only the first vibration mode of the tower explains the structure's response), the displacement of the tower at the top level was determined by the double integration of the acceleration time series. Using a stiffness matrix provided by a simple numerical model developed in the structural analysis software Robot [68], it was possible to determine the equivalent modal force applied at the top level of the tower and the associated bending moment at the section instrumented with strain gages. The method followed to determine the response of the structure in displacement from the measurement of accelerations is further developed in [69,70].

The bending moments variation with respect to the mean value at the base of the tower estimated from accelerations and strains are compared in Figure 9. There is an excellent similarity between the bending moments estimated with the two methods. The error is less than 10% and might be explained by the difficulty in accounting for the exact stiffness of the tower.

Finally, the experimental results are compared with numerical counterparts obtained from a model developed in OpenFAST [26] and calibrated using the methodology described in [71]. OpenFAST is an engineering tool that joins aerodynamics models, hydrodynamics models for offshore structures, control and electrical system (servo) dynamics models, and structural (elastic) dynamics models to enable coupled nonlinear aero-hydro-servo-elastic simulation in the time domain.

The temporal evolution of the bending moments observed in the bottom-instrumented section is presented in Figure 10 for the two main directions (FA and SS), considering two alternative turbine operation scenarios. As shown in the figure, it is possible to verify a good agreement between the numerical (yellow and purple lines, FA (Fast) and SS (Fast)) and experimental (blue and orange lines, FA (sg) and SS (sg)) results. It is important to note that this is just a qualitative comparison. In fact, the simulated wind loads respect the mean and standard deviation observed in the field measurements, but the time series are different. In other words, only the average wind speed and turbulence intensity are the

same for the numerical and experimental results. In both analyzed situations, the mean values and scatter of the FA bending moments are very similar.

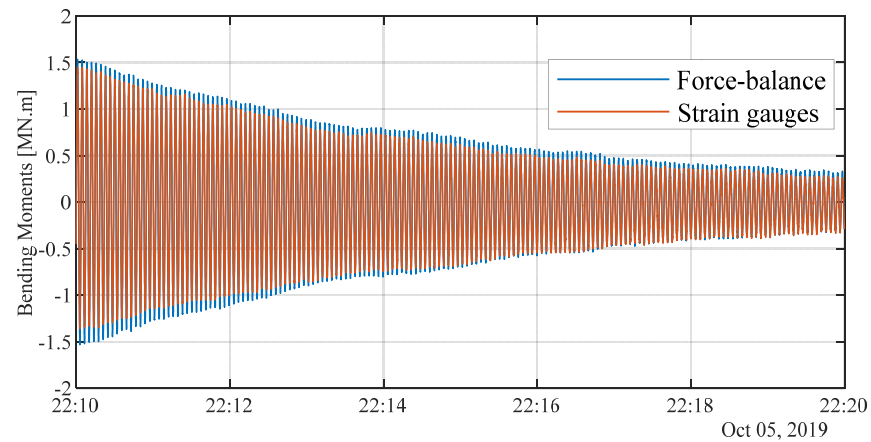


Figure 9. Bending moment variations at the base of the tower estimated from acceleration and strain time series during a rotor stop event.

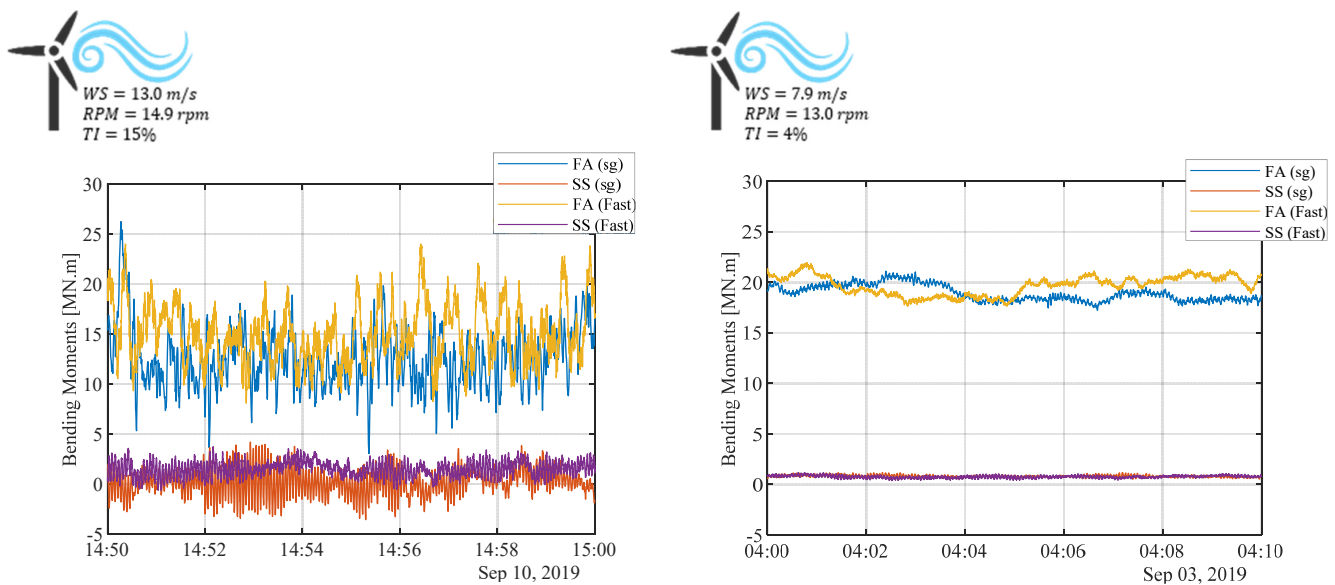


Figure 10. Experimental and numerical bending moments time series for FA and SS directions in the bottom-instrumented section of the tower considering two different operating conditions.

After the calibration and validation of the methodology to estimate the bending moments at the base of the tower from strain measurements, Figure 11a shows the 10 min average bending moment at the tower-instrumented section for the fore–aft direction versus the 10 min average wind speed provided by the SCADA system during normal operation, considering variable levels of turbulence intensity. This figure shows that the drag force acting on the rotor (responsible for the deflection of the tower) increases with the wind speed until reaching the rated rotor rotation speed. Due to the activation of the pitch control to keep the lift force and the rotor speed constant, the value of the drag force reduces as the wind speed increases. It is important to note that for the same values of wind speed, different values of bending moments are obtained because of the effect of turbulence. In fact, the maximum moment decreases as the intensity of the turbulence increases. This behavior is explained by the impact of the wind turbine control algorithms, in particular the pitch control system.

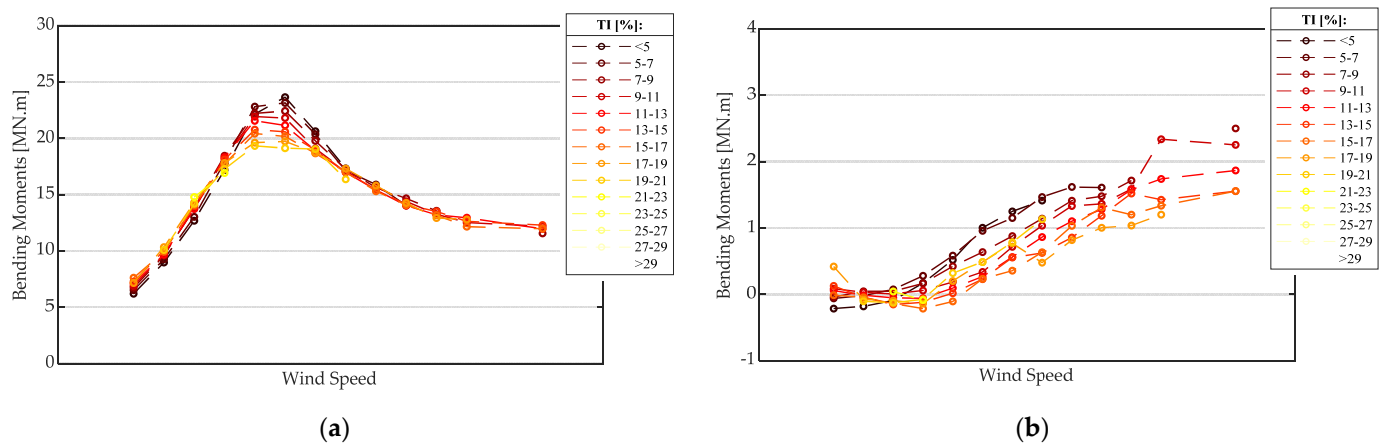


Figure 11. Variation of 10 min average bending moments at the tower base as a function of the wind speed and turbulence intensity, considering normal power production: (a) fore–aft direction, and (b) side-to-side direction (x scale omitted because of confidentiality agreements).

The 10 min average bending moment at the tower instrumented section for the side-to-side direction is represented in Figure 11b as a function of the 10 min average wind speed and of the turbulence intensity. As expected, the bending moments in this direction are significantly lower than the values obtained for the perpendicular direction. The average bending moments increase as the wind speed increases, especially after activation of the pitch control system. Again, for the same wind speed, the bending moment values are higher when the turbulence intensity is lower.

5. Fatigue Assessment of Wind Turbine Tower

To demonstrate the practical applicability of the methodology for the fatigue assessment of wind turbine towers based on strain measurements (described in Section 2), the database acquired in the experimental campaign in the Tocha Wind Farm (introduced in Section 3) was processed according to this methodology. The results presented in this section are based on experimental data obtained between February 2019 and April 2020 (15 months).

In this first analysis, only the damage accumulated during the monitoring period was calculated and at the precise strain measurement position. The instrumented cross-section is close to a horizontal welding, so this detail was used for the selection of the S-N curve. Since the main goal of this work is the presentation of the processing strategy, it was not assured that this be one of the most critical sections of the tower in terms of fatigue design. Note that, in this paper, the extrapolation of the bending moments at a critical location (Section 2.2) and the extrapolation of the fatigue damage in time based on monitored period (Section 2.6) were not performed. These analyses will be performed and discussed in future works.

As mentioned above, before applying the methodology for fatigue assessment, it is necessary to previously define several parameters, such as those that influence the S-N curves or the processing associated with the algorithm used for counting stress cycles. To understand the influence of some relevant parameters on the calculated damage, the following variables will be evaluated independently:

- Window length;
- Rainflow histogram resolution (number of stress bins and stress range);
- S-N curve parameters;
- Strains signal sampling frequency.

The first parameter is the window length of the strain time series used to estimate the stress cycles. The damage was estimated over one-half of the instrumented cross-section using 10 min and 24 h long time series, recorded during 15 months and according to the

S-N curve provided in Eurocode 3. Figure 12a shows the damage calculated from 0° to 180° with 5° intervals considering the two window lengths. The damage obtained with 10 min time series was found to be 11% lower than the damage calculated with 24 h time series. It is verified that the maximum damage in the section occurs for an angle close to the prevailing wind orientation, as demonstrated in Figure 3c.

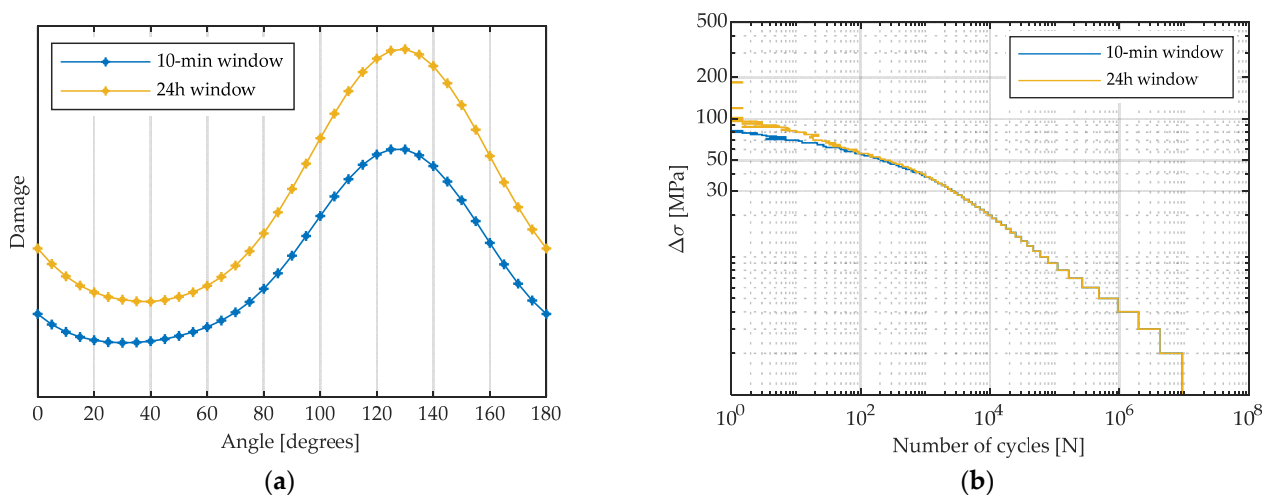


Figure 12. Influence of the window length: (a) damage distribution over half of the section (y scale omitted due to confidentiality agreements); and (b) histogram of the stress cycles.

Figure 12b shows the histogram of the stress cycles obtained for the two window lengths. As shown in the histogram, a relevant difference can be seen between the two curves for the largest stress cycles, starting from 50 MPa. The differences observed can be justified by the uncounted fatigue cycles. In fact, cycle counting allows the capturing of the fatigue cycles within the 10 min datasets, but some other loops are not counted because the algorithm cannot catch low-frequency cycles spanning more than 10 min. These largest cycles can result from changes in wind direction or start-stop events and are only detected when the rainflow-counting algorithm is performed in a large period. Additionally, low-frequency cycles can also be the most damaging, since they always contain the highest range in the variable amplitude signal. In this way, counting multiple 10 min signals has nonconservative effects as they underestimate the cycles with stress variations above 50 MPa.

Sadeghi et al. [72] found differences of 10%, 25%, and 50% between cumulative damage for different wind lengths at a multi-megawatt offshore wind turbine support structure, considering S-N curve with Wöhler exponents of 3, 4, and 5, respectively.

The most obvious solution to overcome this error is to concatenate the segmented time series in the time window of interest. However, this option is undoubtedly time/memory demanding. An approach that significantly reduces calculation time without losing accuracy in the final spectrum histogram was introduced by Marsh et al. [73] and successfully applied by Sadeghi et al. [72]. To obtain the number of cycles per stress level, the 10 min strain time series were processed with the rainflow cycle-counting method [53]. The mean stress was disregarded for the reasons presented in Section 2.1. The number of stress bins and the stress range, which are used in the algorithm, directly influence the calculated damage. Thus, the stress histogram was computed for a stress range of 0 to 500 MPa and considering bins with the amplitude of 1 MPa (500 bins), 2 MPa (250 bins), 4 MPa (125 bins), 7 MPa (71 bins), and 10 MPa (50 bins). Figure 13a shows the relative difference of the calculated damage in the cross-section, considering the 1 MPa bin amplitude as the reference. Figure 13b represents the stress histogram for the 1 MPa, 2 MPa, and 10 MPa amplitude bins.

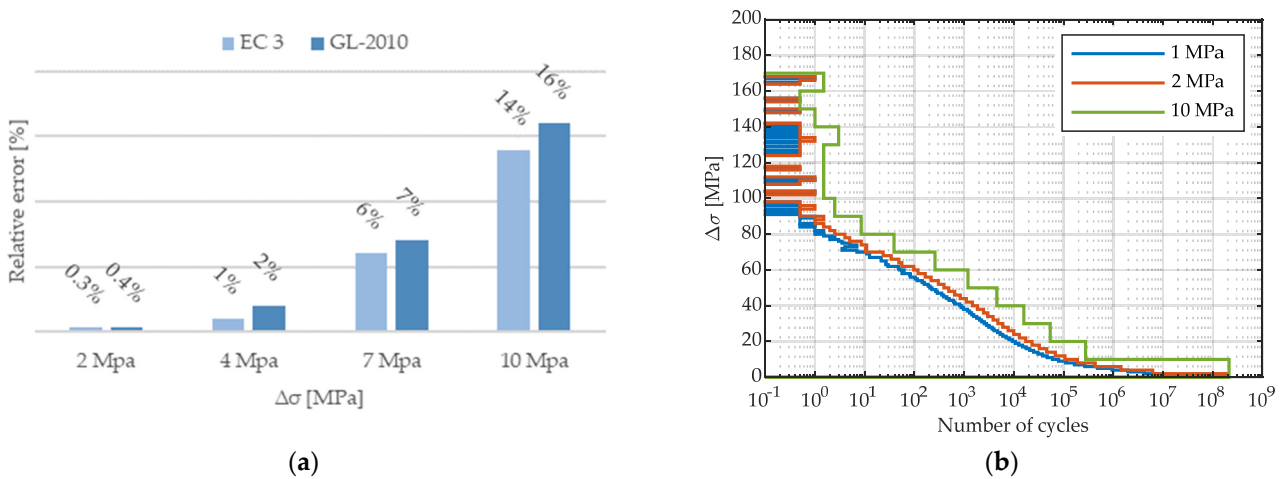


Figure 13. Influence of the rainflow histogram resolution: (a) relative difference of the calculated damage (the 1 MPa bin amplitude is the reference); and (b) stress cycles histogram.

As shown in the figures, there is an increase in accumulated damage as the bin amplitude increases. This is due to the loss of resolution of the stress histogram for the cycles associated with higher stress variation, as shown in Figure 13b. In all the remaining analyses, a bin amplitude of 1 MPa was adopted.

Another important analysis is the influence of the S-N curve parameters on the calculated damage. Figure 14a shows the damage from the 10 min time series along half of the section based on two alternative S-N curves represented in Figure 2 (with and without endurance limit).

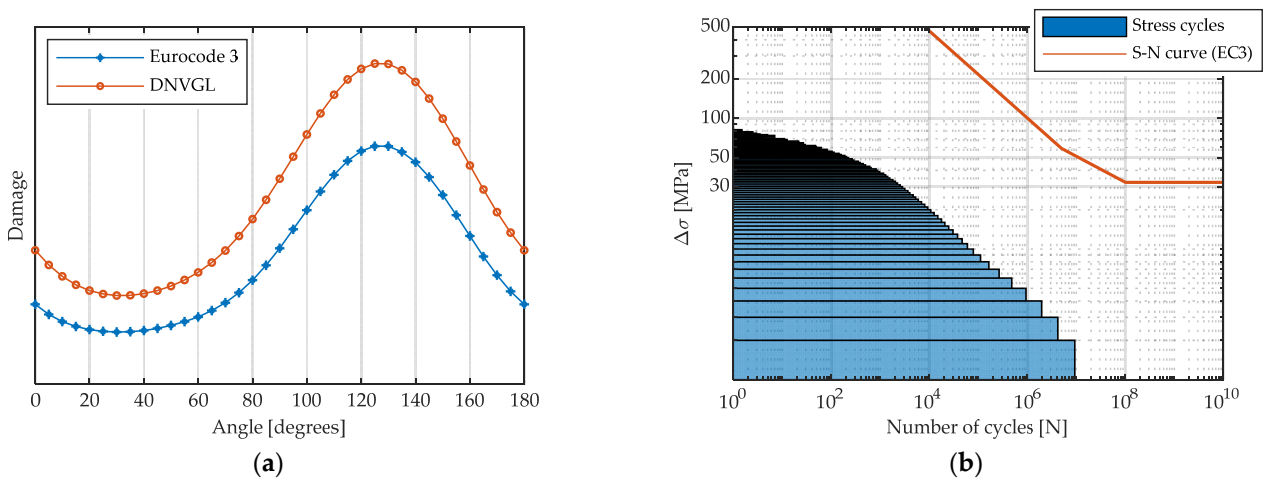


Figure 14. Influence of the S-N curve parameters: (a) damage distribution over the section (y scale omitted due to confidentiality agreements); and (b) histogram of the stress cycles and S-N curve provided by Eurocode 3.

It is possible to verify that the damage calculated with the S-N curve provided in Eurocode 3 (considering endurance limit) is significantly lower (approx. 30%) than the damage calculated with bilinear S-N curve without considering endurance limit. The large percentage of low amplitude stress cycles in the monitored data, as shown in Figure 14b, justifies these results. In fact, this figure shows that 99% of the total identified cycles are below the endurance limit (44 MPa for category details of 80 MPa).

Finally, the influence of the sampling frequency of the acquired strains signal is evaluated. As previously mentioned, this acquisition system is programmed with a sampling

frequency of 50 Hz. In an attempt to reduce the calculation time with the application of the rainflow algorithm, the acquired signal was decimated to 25 Hz and 12.5 Hz.

Three alternatives were followed to decrease the signal sampling frequency. First, the Matlab “decimate” function was directly applied to the signal. In the second alternative, the signal was resampled without the prior application of a low-pass filter (assuming no relevant frequency content in frequencies above one-half of the sampling frequency). Alternatively, the signal was filtered (Chebyshev Type I and Butterworth filters were applied independently) and then resampled to the desired sampling frequency. The basics of low-pass filtering are discussed in [74]. Figure 15 compares the stress cycles as a function of the accumulated damage associated with the four tested alternative preprocessing with the one given by the original signal. The damage was estimated based on the bilinear S-N curve provided in GL-2010.

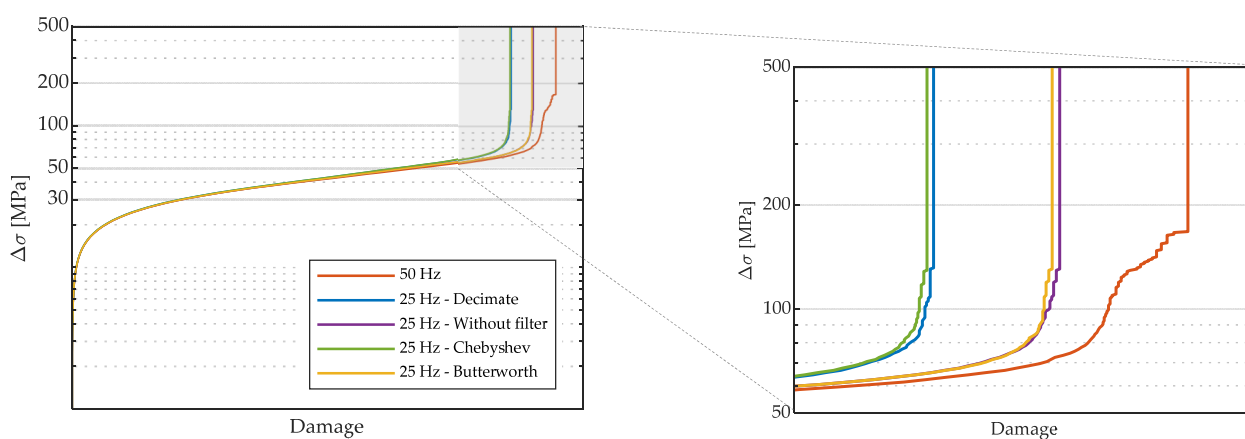


Figure 15. Influence of signal sampling frequency. Stress cycles as a function of the accumulated damage for a sampling frequency of 25 Hz, with zoom (x scale omitted because of confidentiality agreements).

The previous figures allow us to understand the importance of the procedure to be adopted in the resampling of the signal. As shown, the selected method can have a great influence on the total calculated damage. The “decimate” function of the Matlab uses the Chebyshev Type I filter to decimate the signal. For that reason, the results between these two methods are so close.

The application of the Butterworth low-pass filters showed less impact on the estimated damage. These results reflect the importance of the low-pass filter selection. The figures also show the resampling of the signal will always lead to a reduction in the estimated accumulated damage.

The damage distributions over half of the section obtained from all the tested preprocessing methods are presented in Figure 16a. The purple curve is overlapped with the yellow curve and the blue curve with the green curve. Comparing with the damage calculated from the original signal, it is possible to observe a difference of -4.6% for the alternative without filter, and -9.4% and -4.8% considering the Chebyshev Type I and Butterworth filters, respectively.

Figure 16b represents the damage distribution over half of the section calculated according to the bilinear S-N curve provided in GL-2010, adopting a Butterworth filter with two alternative re-sampling rates. The damage calculated with signals with a sampling frequency of 25 Hz and 12.5 Hz were found to be 4.8% and 6.6% lower, respectively, than the damage calculated with the original signal (cumulative damage calculated for the critical angle of the section).

Table 2 shows the relative differences between the accumulated damage at the critical angle of the cross-section of the tower, considering the different sampling methods and sampling frequencies.

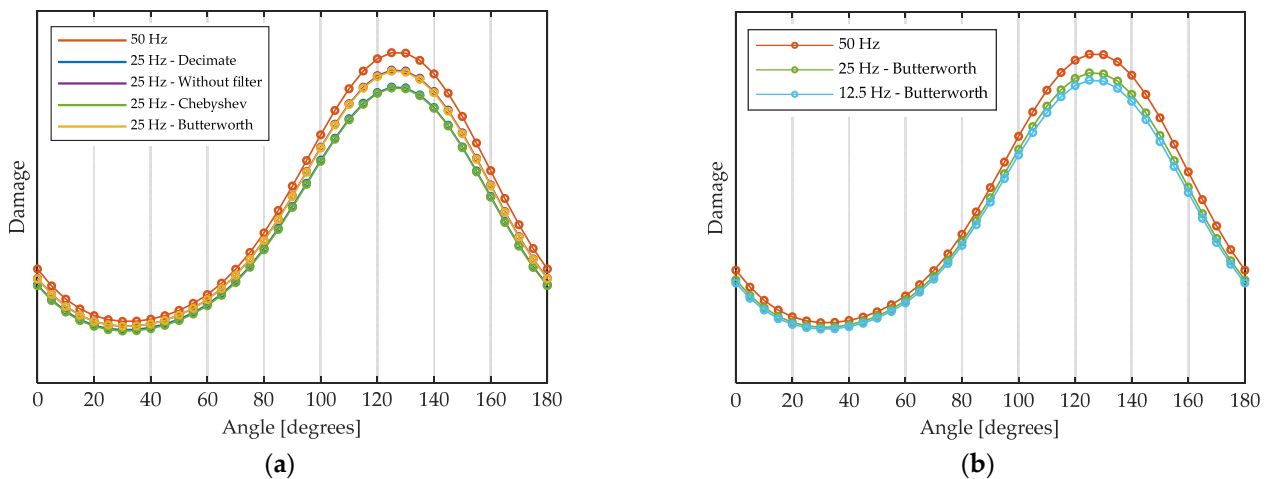


Figure 16. Influence of signal sampling frequency: (a) damage distribution over the section considering tree methods ($f_s = 25$ Hz); and (b) damage distribution over the section for all sampling frequency (Butterworth filter). Y scale omitted because of confidentiality agreements.

Table 2. Relative differences of accumulated damage at the critical angle of the cross section of the tower considering the different sampling methods and sampling frequencies [%].

Method	$f_s = 25$ Hz	$f_s = 12.5$ Hz
Matlab “decimate” function	−8.8	−10.5
Without low-pass filter	−4.6	−6.4
Chebyshev Type I filter	−9.4	−11.0
Butterworth filter	−4.8	−6.6

It is important to note that the results here presented refer to the practical case study of the Tocha Wind Farm. Nevertheless, the majority of the results should be representative of other wind turbine models with natural frequencies within the same range (the vast majority of the current models) and with similar stress ranges observed in the tower sections (which should be fulfilled by different models of well-designed wind turbines). In fact, the extrapolation of the results to other practical cases can only be conditioned by the frequency of occurrence of a certain stress range, which results from different wind conditions in the site.

6. Conclusions

A monitoring layout for measurements of tower mechanical loads was validated over a period of two years. A procedure for fatigue assessment based on a time domain analysis is illustrated with a case study. It is demonstrated that the definition of the type of S-N curves, the window length of the strain time series used to estimate the stress cycles, as well as the rain-flow histogram resolution and strains signal sampling frequency, have a relevant influence on the calculated damage.

The following conclusions can be drawn from this paper:

- Automatic data processing can provide windfarm owners with a real estimation of the fatigue consumption, since the strain measurements allow them to accurately estimate the fatigue damage over the monitoring period for the instrumented tower cross-section.
- The influence of all the used-defined parameters to be adopted in the processing of experimental data for fatigue assessment was quantified.
- Direct strain monitoring allows us to record short events, as well as seasonal variations, that can be used to understand the complex wind turbine behavior under a large

variety of operating conditions. These results are very useful to validate numerical estimates obtained with complex aero-elastic simulation tools, such as FAST.

- The temperature and long-term effects on the strain gauge sensors were quantified for this application and a preprocessing procedure was implemented for their minimization.
- The SCADA data, available with low and high frequency, provides very useful and complementary information regarding the environmental and operational parameters of the instrumented wind turbine. The combination of the SCADA data with a strain monitoring system was very effective for the calculation of the mechanical loads, as well as fatigue wear.
- The more precise operational data provided by the SCADA system with high frequency allow us to detect the short events responsible for the overloading of the structure and the yawing nacelle events, fundamental for strain-sensor calibration.
- The presented literature review on the processing of experimental data for fatigue assessment of wind turbine towers and the illustration of the most relevant processing steps in a case study will certainly contribute to a widespread dissemination of the application of these experimental tools on the management of wind turbine assets.

Regarding the experimental campaign developed at the Tocha Wind Farm, the need to overcome the following main difficulties should be referred to other researchers willing to embrace monitoring projects in wind turbines:

- The difficulty of installing monitoring equipment, mainly conditioned by safety issues, simultaneous availability of technical teams from the owner and manufacturer, and limitation of operating windows to avoid long stops and loss of significant energy production.
- The need of maintenance to ensure the continuous operation of monitoring systems over a long period.
- Measurement interferences mainly associated with sensor drifts and temperature effects, which imply a careful preprocessing of the measured data.

The present paper is part of ongoing research for the development of a fatigue assessment strategy driven purely from in situ measurements on operating wind turbines. Based on the realistic damage calculated on the monitoring period (obtained in the present work), the main goal of the ongoing work is to estimate the remaining lifetime of all individual turbines of a wind farm by instrumenting only a subset of the turbines with a load-monitoring setup.

Author Contributions: J.P. is responsible for the processing of the monitoring data collected at the tower and coordinated the writing of the paper. J.P. and F.M. are responsible for the installation of the monitoring system and for the development of the algorithms for data processing. F.P. is responsible for the development of the numerical models of the onshore-instrumented wind turbine. S.P. supported the development of the algorithms for data processing and the paper writing. F.M. and Á.C. are the main investigators of the project and coordinated the monitoring activities and the preparation of the paper. All authors have read and agreed to the published version of the manuscript.

Funding: This research was funded by PhD Grant SFRH/BD/129688/2017, base funding UID/ECI/04708/2020-CONSTRUCT-Instituto de I&D em Estruturas e Construções funded by national funds through the FCT/MCTES (PIDDAC); this work is also financially supported by national funds through the FCT/MCTES (PIDDAC), under the project PTDC/ECI-EST/29558/2017.

Institutional Review Board Statement: Not applicable.

Informed Consent Statement: Not applicable.

Data Availability Statement: The data presented in this study are available on request from the corresponding author. The data are not publicly available due to confidentiality constraints.

Acknowledgments: The authors would like to acknowledge all the collaboration and support provided by INEGI, the wind turbine manufacturer VESTAS, and the wind turbine owner EDP Renewables.

Conflicts of Interest: The authors declare no conflict of interest.

References

1. Schijve, J. Fatigue of structures and materials in the 20th century and the state of the art. *Int. J. Fatigue* **2003**, *25*, 679–702. [[CrossRef](#)]
2. Ewing, J.A.; Humfrey, J.C.W. The fracture of metals under repeated alternations of stress. *Phil. Trans. R. Soc.* **1903**, *200*, 241–250.
3. Sutherland, H.J. A summary of the fatigue properties of wind turbine materials. *Wind Energy* **2000**, *3*, 1–34. [[CrossRef](#)]
4. Ma, K.-T.; Luo, Y.; Kwan, T.; Wu, Y. *Chapter 6—Fatigue Analysis*; Ma, K.-T., Luo, Y., Kwan, T., Wu, Y., Eds.; Gulf Professional Publishing: Houston, TX, USA, 2019; pp. 115–137.
5. Miner, M.A. Cumulative Damage in Fatigue. *J. Appl. Mech.* **1945**, *12*, 159–164. [[CrossRef](#)]
6. Wöhler, A. Versuche zur Ermittlung der auf die Eisenbahnwagenachsen einwirkenden Kräfte und die Widerstandsfähigkeit der Wagen-Achsen. *Zeitschrift Bauwes.* **1860**, *10*, 160–161.
7. LEE, Y.-L. *Chapter 10—Fatigue Analysis in the Frequency Domain*; Lee, Y.-L., Pan, J.W.O., Hathaway, R.B., Barkey, M.E., Eds.; Butterworth-Heinemann: Burlington, MA, USA, 2005; pp. 369–394.
8. Dirlik, T. *Application of Computers in Fatigue Analysis*; University of Warwick: Coventry, UK, 1985.
9. Zhao, W.; Baker, M.J. On the probability density function of rainflow stress range for stationary Gaussian processes. *Int. J. Fatigue* **1992**, *14*, 121–135. [[CrossRef](#)]
10. Bishop, N.W.M. *The Use of Frequency Domain Parameters to Predict Structural Fatigue*; University of Warwick: Coventry, UK, 1988.
11. van der Tempel, J. *Design of Support Structures for Offshore Wind Turbines*; Technische Universiteit Delft: Delft, The Netherlands, 2006.
12. Bulder, B.H.; van Hees, M.T.; Henderson, A.; Huijsmans, R.H.M.; Pierik, J.T.G.; Snijders, E.J.B.; Wijnants, G.H.; Wolf, M.J. *Study to Feasibility of and Boundary Conditions for Floating Offshore Wind Turbines*; Technical Report No. 2002-CMC-R43; TNO: Delft, Netherlands, 2002.
13. Lee, K.H. *Responses of Floating Wind Turbines to Wind and Wave Excitation*; Massachusetts Institute of Technology: Cambridge, CA, USA, 2005.
14. Adedipe, O.; Brennan, F.; Kolios, A. Review of corrosion fatigue in offshore structures: Present status and challenges in the offshore wind sector. *Renew. Sustain. Energy Rev.* **2016**, *61*, 141–154. [[CrossRef](#)]
15. International Electrotechnical Commission. *IEC 61400-3 Wind Turbines—Part 3: Design Requirements for Offshore Wind Turbines*; International Electrotechnical Commission: Geneva, Switzerland, 2009.
16. International Electrotechnical Commission. *IEC 61400-1 Wind Turbines—Part 1: Design Requirements*; International Electrotechnical Commission: Geneva, Switzerland, 2014.
17. Det Norske Veritas (DNV). *DNV-OS-J101—Design of Offshore Wind Turbine Structures*; Det Norske Veritas: Bærum, Norway, 2011.
18. Germanischer Lloyd (GL). *Guideline for the Certification of Wind Turbines*; Germanischer Lloyd: Hamburg, Germany, 2010.
19. Germanischer Lloyd (GL). *Guideline for the Certification of Offshore Wind Turbines*; Germanischer Lloyd: Hamburg, Germany, 2012.
20. Söker, H. Ermittlung von Ermüdungslasten an großen Windenergieanlagen. *DEWI Mag.* **1996**, *8*, 44–48.
21. Rebelo, C.; Veljkovic, M.; Matos, R.; Silva, L.S.D. Structural monitoring of a wind turbine steel tower—Part II: Monitoring results. *Wind Struct. Int. J.* **2012**, *15*, 301–311. [[CrossRef](#)]
22. Pollino, M.C.; Huckelbridge, A.A. In-situ measurements of fatigue demands on a wind turbine support structure. In Proceedings of the 2012 IEEE Energytech, Cleveland, AL, USA, 29–31 May 2012; pp. 1–5.
23. Botz, M.; Oberländer, S.; Raith, M.; Grosse, C. Monitoring of Wind Turbine Structures with Concrete-Steel Hybrid-Tower Design. In Proceedings of the 8th European Workshop on Structural Health Monitoring (EWSHM), Bilbao, Spain, 5–8 July 2016.
24. Weijtens, W.; Noppe, N.; Verbelen, T.; Iliopoulos, A.; Devriendt, C. Offshore wind turbine foundation monitoring, extrapolating fatigue measurements from fleet leaders to the entire wind farm. *J. Phys. Conf. Ser.* **2016**, *753*, 92018. [[CrossRef](#)]
25. Loraux, C.T. *Long-Term Monitoring of Existing Wind Turbine Towers and Fatigue Performance of UHPFRC under Compressive Stresses*; École Polytechnique Fédérale de Lausanne: Lausanne, Switzerland, 2018.
26. Sprague, M.; Jonkman, J.M.; Jonkman, B. FAST Modular Framework for Wind Turbine Simulation: New Algorithms and Numerical Examples. In Proceedings of the 33rd Wind Energy Symposium, Kissimmee, FL, USA, 5–9 January 2015.
27. Sørensen, J.D.; Sørensen, J. *Wind Energy Systems: Optimising Design and Construction for Safe and Reliable Operation*; Woodhead Publishing: Cambridge, UK, 2011.
28. Veljkovic, M.; Feldmann, M.; Naumes, J.; Pak, D.; Simões, L.; da Silva Rebelo, C. Chapter 9—Wind turbine tower design, erection and maintenance. In *Woodhead Publishing Series in Energy*; Sørensen, J.D., Sørensen, J., Eds.; Woodhead Publishing: Cambridge, UK, 2011; pp. 274–300.
29. Verein Deutscher Ingenieure. *Systematic Calculation of Highly Stressed Bolted Joints—Joints with One Cylindrical Bolt*; VDI guideline; VDI MANUALS: Düsseldorf, Germany, 2015.
30. Pedersen, N.L. On analysis and redesign of bolted L-flanged connections. *Wind Energy* **2017**, *20*, 1069–1082. [[CrossRef](#)]
31. Currie, M.; Saafi, M.; Tachtatzis, C.; Quail, F. Structural integrity monitoring of onshore wind turbine concrete foundations. *Renew. Energy* **2015**, *83*, 1131–1138. [[CrossRef](#)]
32. Pelayo, F.; López-Aenlle, M.; Fernández-Canteli, A.; Cantieni, R. Operational Modal Analysis of Two Wind Turbines with Foundation Problems. In Proceedings of the International Operational Modal Analysis Conference (IOMAC), Istanbul, Turkey, 9–11 May 2011.

33. Jacquelin, E.; Bennani, A.; Hamelin, P. Force reconstruction: Analysis and regularization of a deconvolution problem. *J. Sound Vib.* **2003**, *265*, 81–107. [[CrossRef](#)]
34. Lu, Z.R.; Law, S.S. Force Identification Based on Sensitivity in Time Domain. *J. Eng. Mech.* **2006**, *132*, 1050–1056. [[CrossRef](#)]
35. Jayalakshmi, V.; Lakshmi, K.; Mohan Rao, A.R. Dynamic force reconstruction techniques from incomplete measurements. *J. Vib. Control* **2018**, *24*, 5321–5344. [[CrossRef](#)]
36. Klinkov, M.; Fritzen, C. Wind load observer for a 5MW wind energy plant. In *Structural Dynamics*; Springer: New York, NY, USA, 2011.
37. Fritzen, C.-P.; Kraemer, P.; Klinkov, M. *An Integrated SHM Approach for Offshore Wind Energy Plants BT—Structural Dynamics*; Springer: New York, NY, USA, 2011; Volume 3, pp. 727–740.
38. Erazo, K.; Hernandez, E.M. A model-based observer for state and stress estimation in structural and mechanical systems: Experimental validation. *Mech. Syst. Signal Process.* **2014**, *43*, 141–152. [[CrossRef](#)]
39. Gillijns, S.; De Moor, B. Unbiased minimum-variance input and state estimation for linear discrete-time systems with direct feedthrough. *Automatica* **2007**, *43*, 934–937. [[CrossRef](#)]
40. Lourens, E.; Papadimitriou, C.; Gillijns, S.; Reynders, E.; De Roeck, G.; Lombaert, G. Joint input-response estimation for structural systems based on reduced-order models and vibration data from a limited number of sensors. *Mech. Syst. Signal Process.* **2012**, *29*, 310–327. [[CrossRef](#)]
41. Maes, K.; Smyth, A.W.; De Roeck, G.; Lombaert, G. Joint input-state estimation in structural dynamics. *Mech. Syst. Signal Process.* **2016**, *70–71*, 445–466. [[CrossRef](#)]
42. Papadimitriou, C.; Fritzen, C.-P.; Kraemer, P.; Ntotsios, E. Fatigue predictions in entire body of metallic structures from a limited number of vibration sensors using Kalman filtering. *Struct. Control Health Monit.* **2011**, *18*, 554–573. [[CrossRef](#)]
43. Smyth, A.; Wu, M. Multi-rate Kalman filtering for the data fusion of displacement and acceleration response measurements in dynamic system monitoring. *Mech. Syst. Signal Process.* **2007**, *21*, 706–723. [[CrossRef](#)]
44. Palanisamy, R.P.; Cho, S.; Kim, H.; Sim, S.-H. Experimental validation of Kalman filter-based strain estimation in structures subjected to non-zero mean input. *Smart Struct. Syst.* **2015**, *15*, 489–503. [[CrossRef](#)]
45. Hjelm, H.P.; Brincker, R.; Graugaard-Jensen, J.; Munch, K. Determination of Stress Histories in Structures by Natural Input Modal Analysis. In Proceedings of the XXIII International Modal Analysis Conference (IMAC), Orlando, FL, USA, 31 January–3 February 2005.
46. Avitabile, P.; Pingle, P. Prediction of Full Field Dynamic Strain from Limited Sets of Measured Data. *Shock Vib.* **2012**, *19*, 408919. [[CrossRef](#)]
47. Aenlle, M.L.; Hermanns, L.; Fernández, P.; Fraile, A. Stress estimation in a scale model of a symmetric two story building. In Proceedings of the 5th International Operational Modal Analysis Conference, Guimarães, Portugal, 13–15 May 2013.
48. Iliopoulos, A.; Shirzadeh, R.; Weijtjens, W.; Guillaume, P.; Van Hemelrijck, D.; Devriendt, C. A modal decomposition and expansion approach for prediction of dynamic responses on a monopile offshore wind turbine using a limited number of vibration sensors. *Mech. Syst. Signal Process.* **2016**, *68–69*, 84–104. [[CrossRef](#)]
49. Maes, K.; Iliopoulos, A.; Weijtjens, W.; Devriendt, C.; Lombaert, G. Dynamic strain estimation for fatigue assessment of an offshore monopile wind turbine using filtering and modal expansion algorithms. *Mech. Syst. Signal Process.* **2016**, *76–77*, 592–611. [[CrossRef](#)]
50. Oliveira, G. *Vibration-Based Structural Health Monitoring of Wind Turbines*; Faculty of Engineering of the University of Porto: Porto, Portugal, 2016.
51. Rice, R.C. *Fatigue Design Handbook*; Society of Automotive Engineers: Warrendale, PA, USA, 1988.
52. Veers, P.S.; Veers, P.S.; Winterstein, S.R.; Nelson, D.V.; Cornell, C.A. Variable-Amplitude Load Models for Fatigue Damage and Crack Growth. In *Development of Fatigue Loading Spectra*; Potter, J.M., Watanabe, R.T., Eds.; ASTM International: West Conshohocken, PA, USA, 1989; pp. 172–197.
53. Dowling, N. *Fatigue Failure Predictions for Complicated Stress-Strain Histories*; Journal of materials, Vol.7, No.1, 71–87; 1972.
54. Frendahl, M.; Rychlik, I. Rainflow analysis: Markov method. *Int. J. Fatigue* **1993**, *15*, 265–272. [[CrossRef](#)]
55. Matsuishi, M.; Endo, T. Fatigue of metals subjected to varying stress. *Proc. Kyushu Branch Japan Soc. Mech. Eng.* **1968**, 37–40.
56. Rychlik, I. A new definition of the rainflow cycle counting method. *Int. J. Fatigue* **1987**, *9*, 119–121. [[CrossRef](#)]
57. Amzallag, C.; Gerey, J.P.; Robert, J.L.; Bahuaud, J. Standardization of the rainflow counting method for fatigue analysis. *Int. J. Fatigue* **1994**, *16*, 287–293. [[CrossRef](#)]
58. Glinka, G.; Kam, J.C.P. Rainflow counting algorithm for very long stress histories. *Int. J. Fatigue* **1987**, *9*, 223–228. [[CrossRef](#)]
59. International Electrotechnical Commission. *IEC 61400-13 Wind Turbine Generator Systems—Part 13: Measurement of Mechanical Loads*; International Electrotechnical Commission: Geneva, Switzerland, 2015.
60. DNV GL AS. *DNVGL-ST-0262—Lifetime Extension of Wind Turbines*; Det Norske Veritas: Bærum, Norway, 2016.
61. Det Norske Veritas (DNV). *DNV-RP-C203—Fatigue Design of Offshore Steel Structures*; Det Norske Veritas: Bærum, Norway, 2010.
62. Weijtjens, W.; Noppe, N.; Verbelen, T.; Devriendt, C. Fleet-wise structural health monitoring of (offshore) wind turbine foundations. In Proceedings of the 8th European Workshop on Structural Health Monitoring, Bilbao, Spain, 5–8 July 2016; pp. 5–8.
63. Im, S.; Choung, J. Comparison of Fatigue Provisions in Various Codes and Standards-Part 1: Basic Design S-N Curves of Non-Tubular Steel Members. *J. Ocean Eng. Technol.* **2021**, *35*, 161–171. [[CrossRef](#)]
64. Hübler, C.; Weijtjens, W.; Rolfes, R.; Devriendt, C. Reliability analysis of fatigue damage extrapolations of wind turbines using offshore strain measurements. *J. Phys. Conf. Ser.* **2018**, *1037*, 32035. [[CrossRef](#)]

65. Pacheco, J.; Guimarães, S.; Moutinho, C.; Marques, M.; Matos, J.C.; Magalhães, F. New strategies for optimized structural monitoring of wind farms: Experimental campaign. *Wind Energy Sci.* **2020**, *5*, 983–996. [[CrossRef](#)]
66. Hoffmann, K. *An Introduction to Stress Analysis and Transducer Design Using Strain Gauges*; HBM Test and Measurement: Darmstadt, Germany, 2012.
67. Wind Turbine Specification Report. *HAF Wind Energy Project Report*; Morrison Hershfield Limited: Toronto, ON, Canada, 2012.
68. Autodesk. *Robot Structural Analysis Professional, Version 29.0.05650(x64)*; Autodesk: Mill Valley, CA, USA, 2016.
69. Hjelm, H.P.; Brincker, R.; Graugaard-Jensen, J.; Munch, K. Determination of Stress Histories in Structures by Natural Input Modal Analysis. In Proceedings of the 23rd Conference and Exposition on Structural Dynamics 2005 (IMAC-XXIII), Orlando, FL, USA, 31 January–3 February 2005.
70. Oliveira, G.; Magalhães, F.; Cunha, Á.; Caetano, E. Dynamic monitoring system for utility-scale wind turbines: Damage detection and fatigue assessment. *J. Civ. Struct. Health Monit.* **2017**, *7*, 657–668. [[CrossRef](#)]
71. Pimenta, F.; Branco, C.M.; Teixeira, C.M.; Magalhães, F. Calibration of onshore wind turbine numerical model using experimental data. In Proceedings of the 15th EAWC PhD Seminar on Wind Energy, Nantes, France, 29–31 October 2019.
72. Sadeghi, N.; Robbelein, K.; D'Antuono, P.; Noppe, N.; Weijtjens, W.; Devriendt, C. Fatigue damage calculation of offshore wind turbines' long-term data considering the low-frequency fatigue dynamics. *J. Phys. Conf. Ser.* **2022**, *2265*, 32063. [[CrossRef](#)]
73. Marsh, G.; Wignall, C.; Thies, P.R.; Barltrop, N.; Incecik, A.; Venugopal, V.; Johanning, L. Review and application of Rainflow residue processing techniques for accurate fatigue damage estimation. *Int. J. Fatigue* **2016**, *82*, 757–765. [[CrossRef](#)]
74. Thompson, M.T. *Chapter 14—Analog Low-Pass Filters*; Newnes: Boston, MA, USA, 2014; pp. 531–583.